Journal of Materials Chemistry

Dynamic Article Links

Cite this: *J. Mater. Chem.*, 2011, **21**, 3204

www.rsc.org/materials

PAPER

Microwave-assisted gas/liquid interfacial synthesis of flowerlike NiO hollow nanosphere precursors and their application as supercapacitor electrodes†

Chang-Yan Cao,[ab] Wei Guo,[a] Zhi-Min Cui,[c] Wei-Guo Song*[a] and Wei Cai*[b]

Received 2nd November 2010, Accepted 26th November 2010
DOI: 10.1039/c0jm03749d

A rapid method based on an efficient gas/liquid interfacial microwave-assisted process has been developed to synthesize flowerlike NiO hollow nanosphere precursors, which were then transformed to NiO by simple calcinations. The wall of the sphere is composed of twisted NiO nanosheets that intercalated with each other. Such hollow structure is different from widely reported flowerlike nanostructures with solid cores. An Ostwald ripening mechanism was proposed for the formation of the hollow nanostructures. The products were characterized by X-ray powder diffraction, scanning electron microscopy, transmission electron microscopy, high-resolution TEM, energy-dispersive X-ray analysis, and N_2 adsorption-desorption methods. These flowerlike NiO hollow nanospheres have high surface area of 176 $m^2\ g^{-1}$. Electrochemical properties show a high specific capacitance of 585 F g^{-1} at a discharge current of 5 A g^{-1} and excellent cycling stability, suggesting its promising potentials in supercapacitors.

1. Introduction

The increasing demands for energy and growing concerns about air pollution and global warming have called for intense research on energy storage and conversion from alternative energy sources.[1,2] Electrochemical capacitors (also called supercapacitors) are considered as a promising method for energy storage means due to high power densities and stability.[3] The supercapacitors in general include traditional double-layer supercapacitors and Faradic redox reaction pseudocapacitors. The energy density based on pseudo-Faradic processes is usually many times greater than that of the double-layer supercapacitors.[4–8] Transition metal oxides[6,7] and conductive polymers[9–11] are frequently used as the Faradic redox pseudocapacitors. In particular, supercapacitors based on ruthenium oxide have shown ultrahigh pseudocapacitance and excellent reversibility.[12,13] However, the high cost of ruthenium makes this material unsuitable for commercial applications. Hence, searching for alternative inexpensive electrode materials with good capacitive properties becomes important. Transitional metal oxides, such as NiO,[14–16] $Ni(OH)_2$,[8] Mn_2O_3,[6] *etc.* are reported to be viable candidates. Among them, NiO is of particular interest owing to its high theoretical specific capacitance and low cost.[17]

It has been shown that the electrochemical performance of NiO nanostructures largely depends on its morphology, surface area and the presence of dopants,[18–20] suggesting that the development of controlled synthesis of NiO nanostructures with the desired features is a rational approach for better materials. In the past few years, NiO nanostructures with different structures, such as nanorings,[21] nanoflakes,[17] nanocolumns,[15] nanosheets,[22] nano/microspheres,[16] and hollow nanospheres,[23–25] have been successfully fabricated by a variety of methods. In particular, hollow nanosphere structures have several advantages in adsorption, catalysis and electrochemical property.[26,27] The hollow interior space effectively reduces the mass weight and enhances the spatial dispersion, which results in not only high surface area but also better mass transportation. The most common methods for preparation of NiO hollow nanospheres are template-based ones, which are usually complicated and time-consuming using acid/base erosion or calcinations.[23]

In addition, hollow structures that are composed of compact walls normally do not have large surface area, as the walls are composed of aggregated small particles. Flowerlike hierarchical structures, like Fe_2O_3,[28] CeO_2,[29] and MgO[30] exhibit large surface because their consisted of twisted nanosheets as secondary building block. These building blocks stem from a solid core to form the flowerlike morphology. The overall size of these

[a]*Beijing National Laboratory for Molecular Science, Institute of Chemistry, Chinese Academy of Sciences, Beijing, 100190, P.R. China. E-mail: wsong@iccas.ac.cn; Fax: +86-10-62557908; Tel: +86-10-62557908*

[b]*School of Materials Science and Engineering, Harbin Institute of Technology, Harbin, 150001, P.R. China. E-mail: weicai@hit.edu.cn; Fax: +86-451-86418649; Tel: +86-451-86418649*

[c]*School of Chemistry and Environmental Engineering, Beijing University of Aeronautics and Astronautics, Beijing, 100191, P.R. China*

† Electronic supplementary information (ESI) available: Schematic illustration of the microwave-assisted gas/liquid interfacial setup for the preparation of the flowerlike NiO hollow nanospheres. Energy-dispersive X-ray (EDX) spectroscopic analysis of the typical NiO precursor. TG and DTA curves of flowerlike NiO hollow nanosphere precursors under air atmosphere. TEM images of the NiO precursors obtained at different reaction temperatures. See DOI: 10.1039/c0jm03749d

flowerlike structures is in micron meters. Thus the surface of such structures are usually about 30–80 $m^2 g^{-1}$, which is still not high enough for supercapacitors. If twisted nanosheets can self-assembly into flowerlike hollow spheres at sub-micron meter range, the surface area will be enhanced substantially. However, there are few reports on such materials by a single-step process without using template.

Herein, we report a template-free microwave-assisted gas/liquid interfacial method to synthesize flowerlike NiO hollow nanosphere precursors. It is a combination of hollow structure and hierarchical structure. NiO precursor nanocrystals were self-assembled to nanosheets, which were further self-assembled to curved flowerlike hollow nanospheres. An Ostwald ripening mechanism is proposed to explain the formation of such structure. By calcinations, the NiO precursors were transformed to NiO, which maintain its original morphology. The flowerlike NiO hollow nanospheres show excellent electrochemical properties with specific capacitance of 585 F g^{-1} at a discharge current of 5 A g^{-1} and excellent cycling performance.

2. Experimental

2.1 Materials

Ethylene glycol (EG), ammonia solution (25 wt%) and ethanol were purchased from Beijing Chemicals Co. (Beijing, China). $Ni(acac)_2$ (99%) was obtained from Alfa Aesar. All the materials were used as received without any further purification.

2.2 Synthesis of flowerlike NiO hollow nanospheres

The synthesis process is similar to our previous report of Fe_3O_4 nanocrystals based on a beaker-in-autoclave setup.[31] In a typical procedure, 0.5 mmol $Ni(acac)_2$ dissolved in 5 mL of EG was placed in a beaker. The beaker was then placed into a 70 mL Teflon-lined autoclave that contained 6 mL of ammonia solution. The autoclave was sealed and placed in a programmable microwave oven (MDS-6, Shanghai Sino Microwave Chemistry Technology Co., Ltd.). The oven was heated to 170 °C in 3 min by microwave irradiation and then kept at that temperature for 30 min. After cooling to room temperature, green precipitates were collected as NiO precursors by centrifugation and washed with ethanol for several times. NiO was obtained after calcinations of the NiO precursor in air at 300 °C for 4 h.

2.3 Characterization

X-Ray diffraction (XRD) patterns were obtained with a Rigaku D/max-2500 diffractometer with Cu-Kα radiation ($\lambda = 1.5418$ Å) at 40 kV and 100 mA. The microscopic features of the samples were characterized by field emission scanning electron microscopy (FESEM, JOEL 6701F), transmission electron microscopy (TEM) and high-resolution transmission electron microscopy (HRTEM) (FEI Tecnai F20). The nitrogen adsorption and desorption isotherms were measured on Quantachrome Autosorb AS-1 Instrument. The pore size distributions were derived from the desorption branches of the isotherm with the Barrett-Joyner-Halenda (BJH) model. Thermogravimetric analysis (TGA) data were achieved on a Perkin-Elmer model Pyris 1 TGA system.

2.4 Electrochemical tests

The working electrode was prepared by mixing the electroactive material (NiO, 80 wt%), super-P (10 wt%), and Teflonized acetylene black (TAB) (10 wt%). The mixture was then pressed onto a nickel grid (1 cm^2) and dried at 80 °C in air for 3 h. Each electrode contained about 1–2 mg of electroactive material. The electrochemical performance of the NiO sample was evaluated by using a three-electrode cell with Pt foil as the counter electrode and a saturated calomel electrode (SCE) as the reference electrode in 2 M KOH aqueous solution. Cyclic voltammograms (CVs) were measured on a Parstat 2273 advanced electrochemical system. Galvanostatic charge-discharge tests were carried out on an Arbin BT2000 system in the voltage range of 0–0.45 V (*vs.* SCE) under different current densities.

3. Results and discussions

In our recently report, the beaker-in-autoclave setup is designed to confine the synthesis at the gas/liquid interface inside a sealed space to produce mono-dispersed Fe_3O_4 nanocrystals.[31] We further adopted this method to synthesis NiO nanostructures in the present work. As illustrated by Fig. S1 (ESI†), $Ni(acac)_2$ in EG solution was stored in the beaker, while aqueous ammonia solution was placed in the autoclave liner outside the beaker. At room temperature, the beaker separates the two solutions. During the reaction, ammonia was evaporated and reacted with EG solution of $Ni(acac)_2$ at the gas/liquid interface. However, unlike the formation of mono-dispersed Fe_3O_4 nanocrystals in previous report,[31] flowerlike NiO hollow nanosphere structures are obtained.

Fig. 1a shows the SEM image of the typical sample after microwave irradiation at 170 °C for 30 min. It is composed of many uniform, flowerlike architectures approximately 300 nm in diameter. The detailed morphology of the flowerlike nanostructures is shown in Fig. 1b, which reveal that the entire

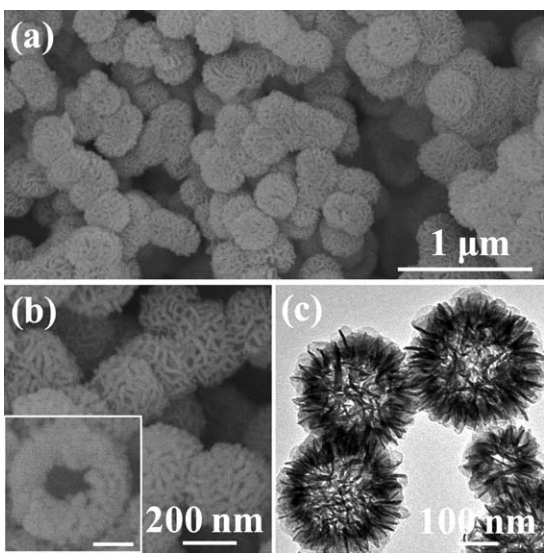

Fig. 1 (a) SEM image of NiO precursor. (b) High magnification SEM image of NiO precursor (inset shows a broken nanosphere, scale bar = 100 nm). (c) TEM image of NiO precursor.

structure of the architecture is composed of numerous twisted nanosheets. These nanosheets connected to each other to form 3D flowerlike structures. Such morphology was reported on several other metal oxides, including Fe_2O_3,[28] CeO_2,[29] MgO.[30] However, for these materials, the flowerlike morphology is generated by twisted nanosheets that are extending out from a solid core. And the overall size of those flowerlike structures is usually in the micron range. The NiO precursors nanostructure in this work is a hollow nanosphere, and the average size of the spheres is only about 300 nm. The hollow structures can be observed by several broken NiO precursors as shown in the inset in Fig. 1b. Furthermore, TEM image (Fig. 1c) confirms that the products have hollow structures.

A series of other measurements were carried out to investigate the as-obtained NiO precursor. The powder XRD pattern (Fig. 2d) shows the strong peak located in the low-angle region (*ca.* 9°), which is similar to those of other metal oxide precursors reported in the literatures,[28,29] though the exact crystal structure of the NiO precursor is yet to be determined. The energy dispersive X-ray (EDX) analysis confirmed that NiO precursor consisted solely of nickel, carbon, and oxygen (Fig. S2, ESI†). From thermogravimetric (TG) analysis (Fig. S3, ESI†), a total weight loss of 10% was observed in the temperature range from 25 to 200 °C because of the removal of water and EG, and weight loss of about 40% in the temperature range from 200 to 700 °C due to the removal of organic species in the precursor by pyrolysis.

To investigate the formation process of flowerlike hollow nanosphere structure, samples prepared at different reaction times are collected and investigated by TEM and XRD. Solid nanospheres are obtained at the initial stage (2 min after microwave heating, Fig. 3a). After 10 min of reaction (Fig. 3b), hollow structure started to appear. After 30 min, complete hollow spheres are obtained (Fig. 3d). XRD patterns of the samples obtained at different reaction times (Fig. 2) display the gradual increase of the crystallinity of the NiO precursors.

On the basis of the above morphology and crystallinity evolution in the time-dependent experiments, it is believed that Ostwald-ripening process should be the main driving force for the formation of these hierarchical architectures. This process is associated with a progressive redistribution of matter from the

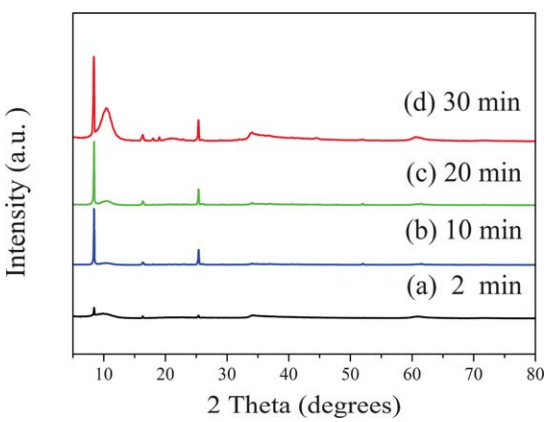

Fig. 2 XRD patterns of the products obtained at different reaction times: (a) 2 min, (b) 10 min, (c) 20 min, and (d) 30 min.

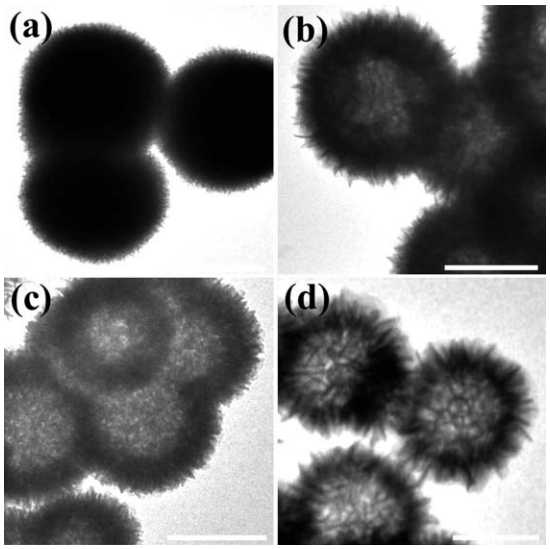

Fig. 3 TEM images of NiO precursors obtained at different reaction times: (a) 2 min, (b) 10 min, (c) 20 min, and (d) 30 min. (Scale bar = 200 nm).

interior to the exterior of the nanospheres.[32–34] At 2 min after microwave heating started, many freshly formed nanoparticles are self-aggregated to form amorphous solid spheres in order to minimize the total surface energy. As the reaction proceeds, the larger crystallites located on the surfaces serve as crystal seeds for the subsequent crystallization process and crystal growth. As a result, the outer crystallites become larger by merging with the smaller crystallites from within, which results in the formation of hollow cores. Finally, after prolonging the reaction time further to 30 min, the whole process is complete.

Such Ostwald-ripening mechanism explains well the effects of reaction temperature on the formation of NiO hollow nanosphere precursors (Fig. S4, ESI†). At lower temperature, for example, 120 °C or 150 °C, only solid nanospheres are obtained. This is because Ostwald-ripening process needs higher temperature to proceed.

Ammonia placed in the autoclave liner outside the beaker was found to play a very important role for the formation of flowerlike NiO hollow nanosphere precursors. In the controlled experiments, only irregular precipitate was collected when pure water was used instead of ammonia solution under the same conditions (Fig. S5, ESI†). According to literatures, EG could serve as a ligand that coordinated with metal ions to form metal alkoxide during the reaction, leaving acidic by-product.[28,29] The increased amount of acid could hamper the formation of metal alkoxide, so that bases are needed to neutralize the acid. In our beaker-in-autoclave setup, ammonia was evaporated into the sealed space above the EG solution of $Ni(acac)_2$. At the gas/liquid interface, ammonia may react with acetylacetone ions, thus prompting the reaction to proceed. In addition, ammonia evaporation could induce higher pressure within the system, which may also benefit the formation of flowerlike NiO hollow nanosphere precursors.

EG was chosen as the solvent because of its high boiling point and strong polarity, as well as its coordinated ability. In a controlled experiment using water as the solvent in the beaker,

we observed aggregates with irregular morphology (Fig. S6, ESI†). This is because ammonia will be dissolved in the water, causing the immediately precipitates of Ni ions.

Thermal decomposition of the precursor is a simple route to obtain corresponding metal oxide. After synthesis of the NiO precursor, we investigated the effect of calcinations on the morphology and crystallization of the products. The XRD pattern (Fig. 4a) of the calcined product matches well with the cubic NiO (JCPDS No. 47-1049). The broaden diffraction peaks indicate the small size of nanocrystals. The average grain size of the nanocrystals is *ca.* 8 nm, as calculated from the width of diffraction peaks using Scherer's formula. SEM image in Fig. 4b shows very similar morphology with the precursor, indicating that calcinations do not change the total nanosphere morphology. TEM image (Fig. 4c) further indicates that NiO remains flowerlike hollow nanosphere structure. Selected-area electron diffraction (SAED) pattern (inset in the Fig. 4c) shows that NiO hollow nanospheres are composed of high crystalline nanocrystals. The lattice fringes in high-resolution TEM (HRTEM) image (Fig. 4d) shows a spacing of 0.21 nm, corresponding to the (200) planes of the NiO.

Nitrogen adsorption study shows that the BET surface area of the flowerlike NiO hollow nanospheres is 176 $m^2\ g^{-1}$ (Fig. 5). Such high surface area is unusual for transition metal oxide materials. A sharp pore size distribution with an average pore size of 4 nm was obtained by BJH method, calculated through the desorption isotherm. These pores are very like due to the void space among the stacked NiO nanocrystals.

The electrochemical performances of the flowerlike NiO hollow nanospheres as electrode materials for supercapacitors were tested using cyclic voltammograms (CVs) and galvanostatic charge-discharge (GCD) in 2 M KOH aqueous solution in the potential range 0–0.45 V *vs.* SCE. Fig. 6a shows the CV curves of the NiO electrode at different scan rates. The shapes of the CV reveal that the capacitance characteristic is very different from that of traditional electric double-layer capacitance in which the

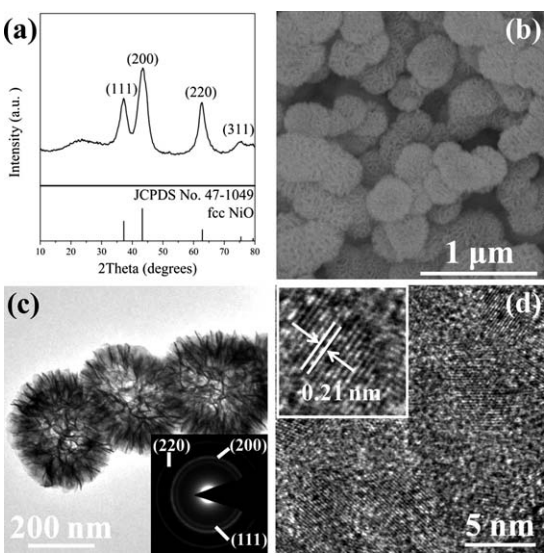

Fig. 4 (a) XRD pattern, (b) SEM image, (c) TEM image (inset: SAED pattern), and (d) HRTEM image of the flowerlike NiO hollow nanospheres.

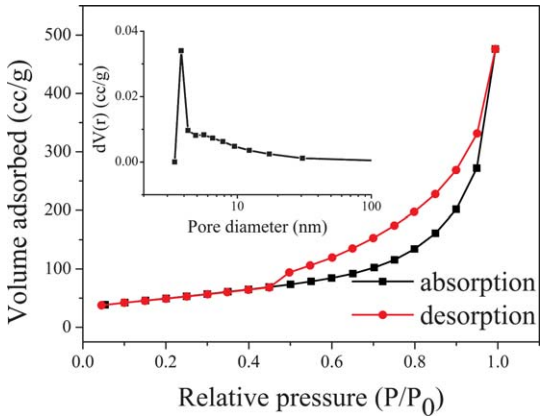

Fig. 5 Nitrogen adsorption-desorption isotherm (with the BJH pore size distribution plot in the inset) of the flowerlike NiO hollow nanospheres.

shape is normally an ideal rectangular shape. A pair of cathodic and anodic peaks is observed in the CV curves. The anodic peak is due to the oxidation of NiO to NiOOH and the cathodic peak is for the reverse process, as shown in eqn (1). This indicates that the observed capacity mainly results from the pseudo-capacitance, which is based on the reversible redox mechanism.

$$NiO + OH^- \underset{\text{discharge}}{\overset{\text{charge}}{\rightleftharpoons}} NiOOH + e^- \qquad (1)$$

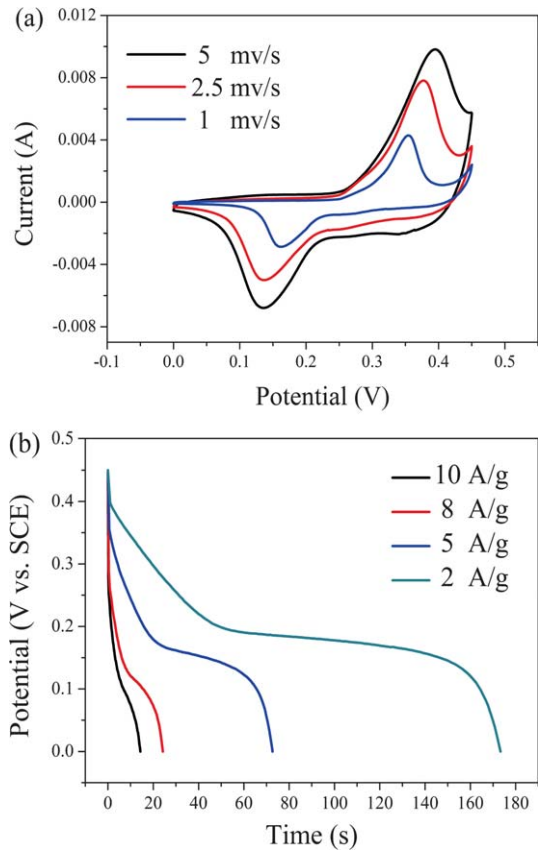

Fig. 6 Electrochemical properties of flowerlike NiO hollow nanospheres in 2 M KOH solution: (a) CV curves at different scan rates; (b) discharging curves at different discharging currents.

Fig. 6b shows the results obtained for the NiO electrode in the potential range of 0–0.45 V in 2 M KOH at various discharging current densities. The specific capacitances were calculated from the galvanostatic discharge curves to be 770, 585, 430, 320 F g^{-1} at discharge current of 2, 5, 8 and 10 A g^{-1}, respectively. As the discharge current increase, a large voltage drop is produced, leading to the capacitance decreases. Despite this, the discharge capacitance at 5 A g^{-1} is still about 76% of that discharge current at 2 A g^{-1}. This high specific capacitance can mainly attributed to the high surface area and hollow nanostructure, which provide effective diffusion channels for the electrolyte ions. In particular, the porous structures can act as "ion reservoirs", which provides steady supply of OH^- ions and ensure that Faradic reactions take place at high current densities for energy storage.[35]

Stability over repeated charge and discharge cycling is critical for supercapacitors in practice. A charge-discharge cycling test was carried out to examine the stability of flowerlike NiO hollow nanospheres electrode at different current densities (2–10 A g^{-1}) between 0–0.45 V (*vs.* SCE) in 2 M KOH electrolyte. As shown in Fig. 7a, increasing the current density from 2 A g^{-1} to 10 A g^{-1} results in the reduction in the specific capacitance from 770 F g^{-1} to 320 F g^{-1}, while a stable cycling performance is maintained. The cyclability of the flowerlike NiO hollow nanospheres was further tested by continuous charge-discharge measurements (Fig. 7b) over 1000 cycles at s current density of 5 A g^{-1}. The specific capacitances increased during the first 60 cycles, which is possibly due to the activation process of the NiO electrode.[15,16] After this process, the specific capacitances were stable at about 585 F g^{-1}, losing only 5% capacitance at the end of the test. Importantly, the Columbic efficiency was nearly 100% through the test (inset in Fig. 7b). In addition, the morphology of flowerlike NiO hollow nanospheres did not change after charge-discharge cycles (Fig. S7, ESI†). These results demonstrate the high specific capacitance and excellent cycling property of the flowerlike NiO hollow nanosphere material for high-performance electrochemical pseudocapacitors.

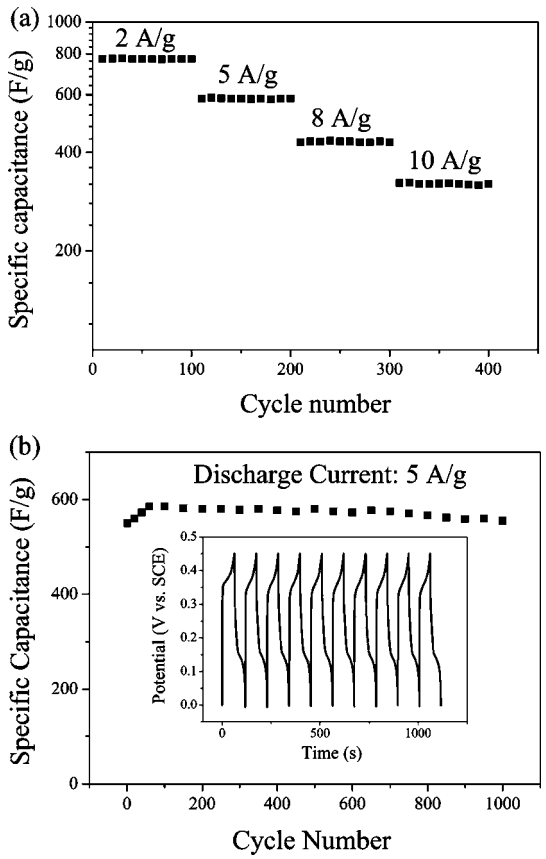

Fig. 7 Cycling performance of as-prepared flowerlike NiO hollow nanospheres electrode in 2 M KOH electrolyte: (a) at different current densities; (b) at a discharge current of 5 A g^{-1} (the inset is the charge/discharge curves of the NiO electrode).

4. Conclusions

In summary, flowerlike NiO hollow nanosphere precursors were produced by a microwave-assisted gas/liquid interfacial method. This is a rapid and template-free method. An Ostwald ripening mechanism was proposed to explain the formation of hollow nanostructure. By calcinations, the NiO precursors were transformed to NiO, which maintain its original morphology. These flowerlike NiO hollow nanospheres showed high specific capacitance of 585 F g^{-1} at a discharge current of 5 A g^{-1} and excellent cycling stability.

Acknowledgements

We thank the financial supports from the National Natural Science Foundation of China (NSFC 50725207, 20873156, 20821003), Ministry of Science and Technology (MOST 2007CB936400, 2009CB930400), Excellent Youth Foundation of Heilongjiang Province of China (No. JC200715), and the Chinese Academy of Sciences.

Notes and references

1 A. S. Arico, P. Bruce, B. Scrosati, J.-M. Tarascon and W. V. Schalkwijk, *Nat. Mater.*, 2005, **4**, 366–377.
2 Y. G. Guo, J. S. Hu and L. J. Wan, *Adv. Mater.*, 2008, **20**, 2878–2887.
3 P. Simon and Y. Gogotsi, *Nat. Mater.*, 2008, **7**, 845–854.
4 R. Liu and S. B. Lee, *J. Am. Chem. Soc.*, 2008, **130**, 2942–2943.
5 K. R. Prasad, K. Koga and N. Miura, *Chem. Mater.*, 2004, **16**, 1845–1847.
6 C. Yu, L. Zhang, J. Shi, J. Zhao, J. Gao and D. Yan, *Adv. Funct. Mater.*, 2008, **18**, 1544–1554.
7 T. Zhu, J. S. Chen and X. W. Lou, *J. Mater. Chem.*, 2010, **20**, 7015–7020.
8 H. Wang, H. S. Casalongue, Y. Liang and H. Dai, *J. Am. Chem. Soc.*, 2010, **132**, 7472–7477.
9 M. E. Roberts, D. R. Wheeler, B. B. McKenzie and B. C. Bunker, *J. Mater. Chem.*, 2009, **19**, 6977–6979.
10 Y. Fang, J. Liu, D. J. Yu, J. P. Wicksted, K. Kalkan, C. O. Topal, B. N. Flanders, J. Wu and J. Li, *J. Power Sources*, 2010, **195**, 674–679.
11 K. Zhang, L. L. Zhang, X. S. Zhao and J. Wu, *Chem. Mater.*, 2010, **22**, 1392–1401.
12 R. R. Bi, X. L. Wu, F. F. Cao, L. Y. Jiang, Y. G. Guo and L. J. Wan, *J. Phys. Chem. C*, 2010, **114**, 2448–2451.
13 Y. F. Ke, D. S. Tsai and Y. S. Huang, *J. Mater. Chem.*, 2005, **15**, 2122–2127.
14 X. Wang, L. Li, Y. g. Zhang, S. Wang, Z. Zhang, L. Fei and Y. Qian, *Cryst. Growth Des.*, 2006, **6**, 2163–2165.
15 X. Zhang, W. Shi, J. Zhu, W. Zhao, J. Ma, S. Mhaisalkar, T. Maria, Y. Yang, H. Zhang, H. Hng and Q. Yan, *Nano Res.*, 2010, **3**, 643–652.
16 C. Yuan, X. Zhang, L. Su, B. Gao and L. Shen, *J. Mater. Chem.*, 2009, **19**, 5772–5777.
17 J. W. Lang, L. B. Kong, W. J. Wu, Y. C. Luo and L. Kang, *Chem. Commun.*, 2008, 4213–4215.

18 W. Xing, F. Li, Z.-f. Yan and G. Q. Lu, *J. Power Sources*, 2004, **134**, 324–330.
19 F. Jiao, A. H. Hill, A. Harrison, A. Berko, A. V. Chadwick and P. G. Bruce, *J. Am. Chem. Soc.*, 2008, **130**, 5262–5266.
20 T. Y. Wei, C. H. Chen, H. C. Chien, S. Y. Lu and C. C. Hu, *Adv. Mater.*, 2010, **22**, 347–351.
21 J. H. Liang and Y. D. Li, *Chem. Lett.*, 2003, **32**, 1126–1127.
22 Z. H. Liang, Y. J. Zhu and X. L. Hu, *J. Phys.Chem. B*, 2004, **108**, 3488–3491.
23 X. Sun, J. Liu and Y. Li, *Chem.–Eur. J.*, 2006, **12**, 2039–2047.
24 X. Song and L. Gao, *J. Phys. Chem. C*, 2008, **112**, 15299–15305.
25 Y. Wang, Q. Zhu and H. Zhang, *Chem. Commun.*, 2005, 5231–5233.
26 C. Y. Cao, Z. M. Cui, C. Q. Chen, W. G. Song and W. Cai, *J. Phys. Chem. C*, 2010, **114**, 9865–9870.
27 X. W. Lou, L. A. Archer and Z. Yang, *Adv. Mater.*, 2008, **20**, 3987–4019.
28 L. S. Zhong, J. S. Hu, H. P. Liang, A. M. Cao, W. G. Song and L. J. Wan, *Adv. Mater.*, 2006, **18**, 2426–2431.
29 L. S. Zhong, J. S. Hu, A. M. Cao, Q. Liu, W. G. Song and L. J. Wan, *Chem. Mater.*, 2007, **19**, 1648–1655.
30 S. W. Bain, Z. Ma, Z. M. Cui, L. S. Zhang, F. Niu and W. G. Song, *J. Phys. Chem. C*, 2008, **112**, 11340–11344.
31 Z. M. Cui, L. Y. Jiang, W. G. Song and Y. G. Guo, *Chem. Mater.*, 2009, **21**, 1162–1166.
32 X. Lou, Y. Wang, C. Yuan, J. Lee and L. Archer, *Adv. Mater.*, 2006, **18**, 2325–2329.
33 H. G. Yang and H. C. Zeng, *J. Phys. Chem. B*, 2004, **108**, 3492–3495.
34 H. C. Zeng, *J. Mater. Chem.*, 2006, **16**, 649–662.
35 D. W. Wang, F. Li, M. Liu, G. Lu and H. M. Cheng, *Angew. Chem., Int. Ed.*, 2008, **47**, 373–376.